NANO LETTERS

pubs.acs.org/NanoLett

Letter

Coherent Control of Topological States in an Integrated Waveguide Lattice

Alexey O. Mikhin, Viktoriia Rutckaia, Roman S. Savelev, Ivan S. Sinev, Andrea Alù, and Maxim A. Gorlach*

Cite This: *Nano Lett.* 2023, 23, 2094–2099

Read Online

ACCESS | Metrics & More | Article Recommendations | Supporting Information

ABSTRACT: Topological photonics holds the promise for enhanced robustness of light localization and propagation enabled by the global symmetries of the system. While traditional designs of topological structures rely on lattice symmetries, there is an alternative strategy based on accidentally degenerate modes of the individual meta-atoms. Using this concept, we experimentally realize topological edge state in an array of silicon nanostructured waveguides, each hosting a pair of degenerate modes at telecom wavelengths. Exploiting the hybrid nature of the topological mode, we implement its coherent control by adjusting the phase between the degenerate modes and demonstrating selective excitation of bulk or edge states. The resulting field distribution is imaged via third harmonic generation showing the localization of topological modes as a function of the relative phase of the excitations. Our results highlight the impact of engineered accidental degeneracies on the formation of topological phases, extending the opportunities stemming from topological nanophotonic systems.

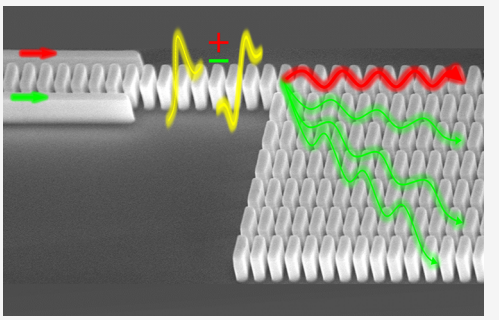

KEYWORDS: *topological photonics, topological edge states, subwavelength grating waveguides, integrated photonic circuits, coherent control*

Topological photonics provides a promising avenue to manipulate light in engineered nanostructures by creating disorder-robust edge or interface states immune to back-scattering at sharp bends and defects.[1−3] The first approaches to tailor such states have been relying on broken time-reversal symmetry by applying an external magnetic bias in magneto-optical materials.[4−6] This strategy, however, faces practical limitations, which have been inspiring a search for alternative time-reversal-invariant platforms,[7−11] such as crystalline topological metamaterials,[11−19] particularly appealing for its experimental accessibility.

In crystalline topological systems, the nontrivial topology of the bands and the associated edge or interface states originate due to the special choice of lattice symmetries that ensure topological degeneracies (e.g., Dirac points) as well as the opening of topological bandgaps for suitable lattice parameters. Prominent examples are one-dimensional (1D) zigzag arrays,[20−25] 2D breathing honeycomb,[11,13] and breathing kagome[26−28] lattices. However, because lattice geometries are challenging to modify dynamically, the topological properties of such systems, e.g., the existence of topological states and their localization length, are difficult to control in real time.

To overcome this limitation, it has recently been suggested to utilize the accidental degeneracy of modes in the individual meta-atoms of a simple lattice.[29,30] In such case, the interference of the near fields of the degenerate modes can regulate the coupling between neighboring meta-atoms, while the detuning between these modes controls the topological transitions.[29−31] Experimental demonstrations of this strategy to create topological structures at the nanoscale have remained elusive so far.

In this Letter, we implement this approach experimentally realizing an integrated optical structure based on an array of multimode nanostructured waveguides that supports topological edge state in the telecom range. By optimizing the design of the waveguides, we ensure that they host a pair of modes with the same propagation constants but different symmetry of the near-field profiles (Figure 1a). Such accidental degeneracy is crucial for the formation of a topological phase and the emergence of topological edge states. In contrast to the traditional implementations of topological physics, these modes have hybrid origin being a superposition of two waveguide modes with different symmetry of the near field. As we demonstrate, this feature enables a coherent control of the topological edge state.

Received: October 25, 2022
Revised: March 6, 2023
Published: March 10, 2023

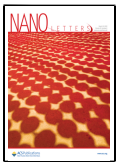

https://doi.org/10.1021/acs.nanolett.2c04182
Nano Lett. 2023, 23, 2094−2099

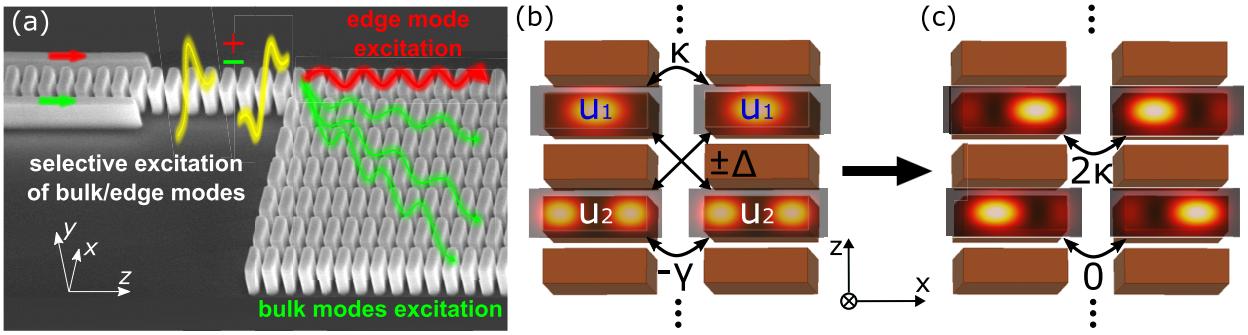

Figure 1. (a) Scanning electron microscopy image (SEM) of the fabricated structure with schematic profiles of the near-field distributions for two quasi-degenerate modes of the structured waveguide (yellow curves). Depending on the relative phase difference with which these modes are initiated through the directional couplers, either a topological edge mode (red curve) or bulk modes (green curves) of the waveguide array are excited. (b, c) Schematic of the field distributions for (b) even (u_1) and odd (u_2) modes of two uncoupled neighboring waveguides (c) modes of the coupled waveguides in the limit of $\kappa = \gamma = \Delta$. Hybridization of the modes gives rise to asymmetric field profiles.

Generally, the goal of coherent control phenomena is to tailor the relative phases of multiple excitation signals to control the response of the system in real time.[32−34] In photonics, this is often achieved through the interference of excitations from multiple ports.[35,36] In our case, coherent control is ensured by manipulating the relative phase between two waveguide modes, which allows us to switch between the excitation of edge and bulk modes of the lattice. To image the modes of the fabricated waveguide structure, we excite it with short laser pulses and collect the third harmonic signal, which provides a sensitive tool to detect the localization.

The key ingredient necessary to obtain the topological features in our setup is the degeneracy of two modes with distinct symmetries of their near-field distributions. To clarify the mechanism of the mode hybridization in the waveguide lattice, we consider two coupled waveguides assuming the evanescent coupling between the modes and applying the tight-binding model. The amplitudes of the modes are denoted as $u_{1,2}^{(l,r)}$, where the lower indices 1 and 2 denote symmetric and antisymmetric modes, while the upper indices l and r stand for the left and right waveguides, respectively. κ and $-\gamma$ denote the coupling constants between a pair of even or pair of odd modes in the adjacent waveguides, respectively, whereas $\pm\Delta$ is the coupling between the modes of different parity (see Figure 1b and the Supporting Information for details and convention on the phase choice).

To reveal the physics underlying the localized modes, we examine the limiting case $\Delta = \kappa = \gamma$ and switch to the basis $u_{\pm} = (u_1 \pm u_2)/\sqrt{2}$. Rewriting coupled mode theory in such a basis, we recover only one nonvanishing coupling 2κ between the states $u_{-}^{(l)}$ and $u_{+}^{(r)}$ (upper profiles in Figure 1c), while the remaining two modes $u_{+}^{(l)}$ and $u_{-}^{(r)}$ (lower profiles in Figure 1c) are uncoupled from each other, and hence their propagation constants remain unchanged by the interaction in the tight-binding limit. Note that the coupling of the latter pair of modes remains suppressed even in the absence of parameter fine-tuning.

In a finite array of N waveguides, the described hybridization of the modes leads to the formation of the edge-localized states. Similarly to the case of two coupled waveguides, the linear combination of two degenerate modes in the leftmost (rightmost) edge waveguide $u_{+}^{(l)}$ ($u_{-}^{(r)}$) features the hot spot at the edge of the structure and is decoupled from the rest of the lattice, thus ensuring the presence of two edge states simultaneously. The tight-binding analysis of the infinite array shows a complete gap in the spectrum of the propagation constants which can be shown to be topological by the direct evaluation of the Zak phase (see the Supporting Information for details). The outlined picture holds even if κ, γ, and Δ are not equal to each other as long as κ and γ coupling constants have the same sign.

Because each of the waveguides in our structure has two modes associated with it, the array of N waveguides can be mapped onto $2 \times N$ ladder (Supporting Information). However, the topological properties of our system are protected by the 1D topological invariant which distinguishes it from the concept of topological structures in synthetic dimensions.[37,38]

To achieve the desired functionality and support our qualitative reasoning, we design subwavelength structured waveguides etched from crystalline silicon on sapphire substrate as shown in Figure 2a. Such nanostructuring of the waveguides provides the periodic permittivity modulation essential for dispersion engineering of the two modes.[39] In our case, by tuning the width of the gaps cut in an initially homogeneous silicon ridge waveguide, we tailor the dispersion of the two modes of interest—a fundamental hybrid quasi-HE_{11} mode with dominant x component of the magnetic field and the first quasi-TE_{01} mode with dominant z component of the magnetic field along the waveguide axis. Substantially different strengths of the z-component of the electric field for these modes result in different dispersion shifts as we vary the gap width.[40] By optimizing the geometric parameters, we achieve an intersection of the dispersion branches of these modes in the telecom range $\lambda \approx 1.55$ μm, as shown by the green curves in Figure 2b (see the Supporting Information for details). The respective distributions of electric field for those modes are shown in Figure 2c being qualitatively the same in all studied wavelength range.

Performing full-wave numerical simulation of the finite array, we recover the bands of waveguide modes shown by shaded areas in Figure 2b. The blue areas correspond to the bands formed by the two modes of interest with dominant polarization of the magnetic field in the plane of the substrate, while the gray area corresponds to an additional mode with dominant out-of-plane polarization of the magnetic field. Because of the presence of the substrate, the modes with

https://doi.org/10.1021/acs.nanolett.2c04182
Nano Lett. 2023, 23, 2094−2099

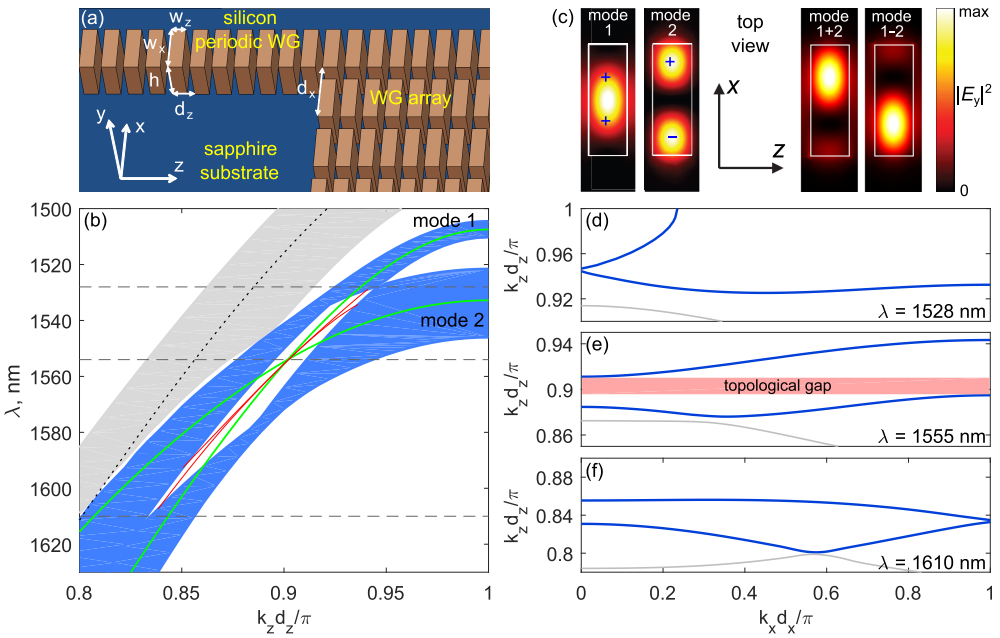

Figure 2. (a) Schematic of a silicon waveguide array with extended edge waveguide on a sapphire substrate. The geometrical parameters of the structure are h = 600 nm, w_x = 605 nm, w_z = 205 nm, d_x = 790 nm, and d_z = 300 nm. (b) Dispersion of the three modes of the individual waveguide with the lowest frequency (solid green and black dotted curves), and the dispersion bands of the waveguide array (shaded areas) obtained with full-wave numerical simulations. Two red curves show the dispersion of two nearly degenerate edge modes in the array of seven waveguides. (c) Intensity distributions of the y component of the electric field $|E_y|^2$ in the unit cell of the individual periodic waveguide. Left two panels: $|E_y|^2$ for hybrid quasi-HE_{11} and quasi-TE_{01} modes, respectively, at the wavelength of their intersection; + and − indicate the phase of the field. Right two panels: $|E_y|^2$ for the superposition of two modes $|E_{y1} \pm E_{y2}|^2$. The similar field distributions arise at other wavelengths in the studied spectral range. (d–f) Calculated dependence $k_z(k_x)$ for the periodic array at three representative wavelengths λ marked in (b) by the horizontal dashed lines.

different polarizations mix with each other, becoming hardly distinguishable at long wavelengths $\lambda > 1600$ nm.

To access the topological properties of the designed structure, we examine the spectrum of the propagation constants k_z versus Bloch wavenumber k_x. If the wavelength of operation λ is close to the target value 1.55 μm, the spectrum of the propagation constants features a gap (Figure 2e), and the associated topological invariant—Zak phase—acquires a nonzero value. In the absence of perfect mode degeneracy, the two types of modes hybridize less, and hence the mechanism of the mode interference becomes less effective. In particular, our tight-binding calculations (see the Supporting Information) suggest that upon reaching the critical detuning δk between the propagation constants of the two waveguide modes the bandgap closes, and the topological protection is lost (Figure 2d,f). As a consequence, the topological edge states disappear. To verify this, we simulate a finite array of seven waveguides numerically and reveal the edge states with the dispersion shown in Figure 2b by the red curves. The edge states arise within approximately 50 nm wavelength interval. Hence, by sweeping the wavelength of operation, one can readily adjust the width of the gap in the spectrum of propagation constants k_z and control the localization of the topological mode, switching it from tight localization at the edge to complete delocalization over the entire array.

An interesting feature of the predicted topological modes evident already from our qualitative analysis is their hybrid nature: they are the superposition of symmetric $\mathbf{E}_1$ and antisymmetric $\mathbf{E}_2$ modes of the individual waveguides, $\mathbf{E}_{edge} \approx \mathbf{E}_1 + \mathbf{E}_2$. As a result, the near field of the edge modes is strongly asymmetric and it almost vanishes in the direction toward the bulk of the waveguide lattice (Figure 2c) which effectively decouples the edge state from the rest of the array. In contrast, the field of the bulk states characterized by a π phase difference between the waveguide modes, $\mathbf{E}_{bulk} \approx \mathbf{E}_1 - \mathbf{E}_2$, is strongly suppressed at the edge of the array being coupled to the rest of the lattice.

The hybrid nature of the topological mode provides a useful tool for its coherent control. Because the fields of bulk and edge modes are strongly asymmetric relative to the center of the edge waveguide, they can be selectively excited by launching the excitation through the auxiliary homogeneous single-mode bus waveguide (SMWG) placed either from the left or from the right edge from the edge waveguide (Figure 1a). Here, the width of the SMWG is adjusted in such a way that the dispersion of its fundamental mode crosses the intersection point of the two modes of the multimode waveguide.

To quantify the degree of coherent control of our system, we simulate the field distribution at the output facet of the array for the various relative phases ϕ between the two waveguide modes launched into the edge waveguide. To achieve that, we assume that the left and right single-mode bus waveguides are excited simultaneously with $\pi/2$ phase shift between the excitations: $\mathbf{E}_{tot} = \mathbf{E}_r \cos\frac{\phi}{2} + i\mathbf{E}_l \sin\frac{\phi}{2}$. Because excitations of right and left couplers translate into $\mathbf{E}_1 + \mathbf{E}_2$ and $\mathbf{E}_1 - \mathbf{E}_2$ superpositions of the waveguide modes, the output field reads $\mathbf{E}_{tot} \propto \mathbf{E}_1 e^{i\phi/2} + \mathbf{E}_2 e^{-i\phi/2}$ which is indeed a superposition of the two waveguide modes with ϕ phase difference between them. Numerical results presented in Figure 3 confirm our expectation showing efficient localization of light for in-phase excitation of $\mathbf{E}_1$ and $\mathbf{E}_2$ and almost complete delocalization for the out-of-phase excitation.

https://doi.org/10.1021/acs.nanolett.2c04182
Nano Lett. 2023, 23, 2094−2099

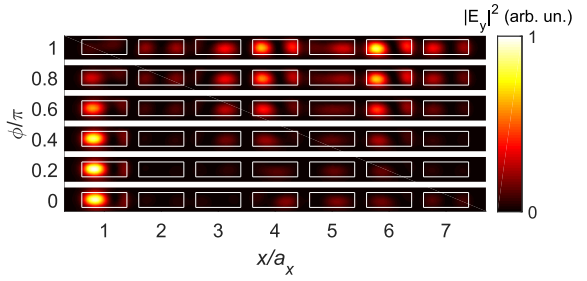

Figure 3. Distribution of the field $|E_y|^2 = |E_r \cos(\phi/2) + iE_l \sin(\phi/2)|^2$ in the array of seven waveguides at the output unit cell for the different values of ϕ. E_r and E_l denote the electric fields excited in the waveguide array via right or left directional coupler, respectively.

The designed array of nanostructured waveguides was fabricated on a silicon on sapphire substrate with a 600 nm device layer using standard CMOS-compatible fabrication techniques (see the Methods section). The scheme of the experiment and the optical image of the fabricated device are provided in Figures 4a and 4b, respectively. To excite the structure from the far field, we have added linear tapers and fully etched grating couplers to the designed SMWGs.

As a convenient tool to visualize the field of bulk and edge states, we exploit the third-harmonic generation (THG) process. Because the third harmonic signal has the wavelength three times smaller than the fundamental wave, this technique provides excellent spatial resolution to capture the finest details of the field distribution allowing also to outcouple light from the waveguide structure for the far-field detection. In addition, because the intensity of the third harmonic scales as the cube of intensity of the fundamental wave, third harmonic spectroscopy is especially suitable for detecting localized states.[18,24]

The scheme of the experimental setup is shown in Figure 4a. Linearly polarized laser pulses with magnetic field oriented along the grating bars (TM polarization) are focused on one of the grating couplers marked by blue in Figure 4b from the substrate side. The pulses are generated by an optical parametric amplifier, which allows us to tune the excitation wavelength within a broad spectral range. Light coupled to the planar waveguide via the grating passes through the taper region and excites one of the SMWGs. The energy from the SMWG is further transferred to the extended structured waveguide (marked by green in Figure 4b) in the form of in-phase or out-of-phase superposition of the two waveguide modes depending on the chosen excitation port: right (1) or left (2) coupler. The area of the sample containing the directional coupler and the waveguide array is then imaged on a CCD camera. The detected third harmonic signal allows us to visualize the propagation of the modes in the waveguide array.

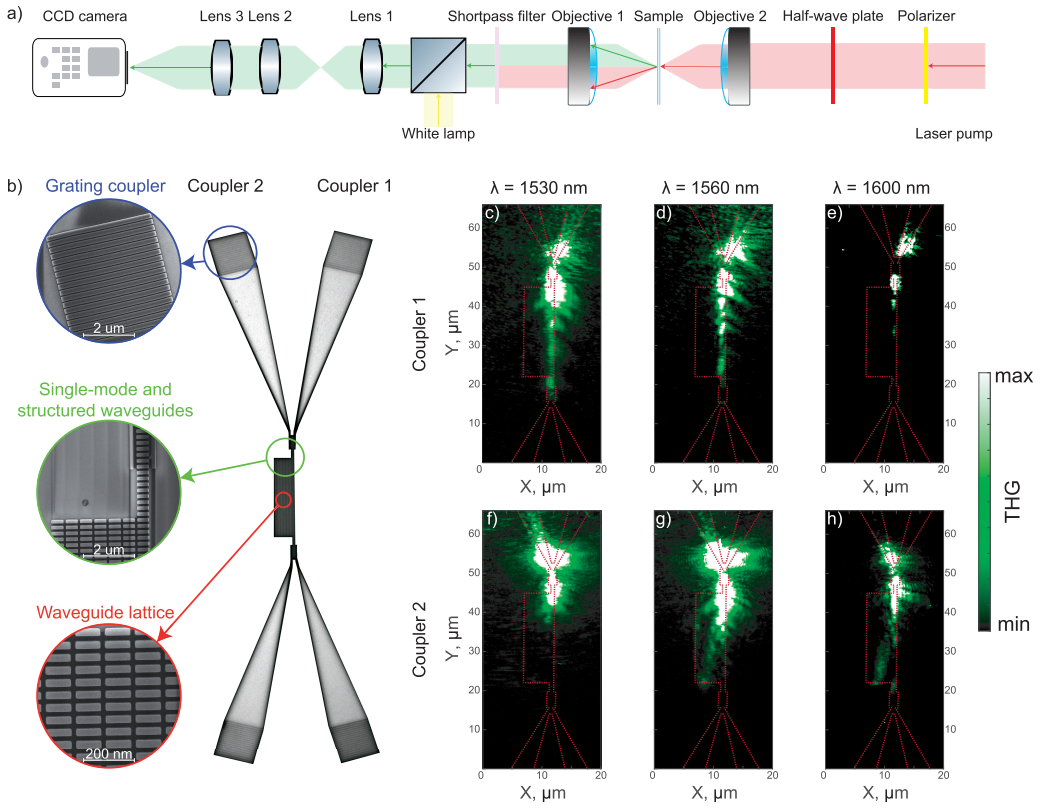

Figure 4. (a) Scheme of the experimental setup for third harmonic measurements in the transmission geometry. The red arrow indicates the excitation laser path, the green arrow indicates the third harmonic signal, and the yellow arrow indicates the white lamp for the visualization of the sample. Linearly polarized light is focused on the grating coupler through the objective 2, and the third harmonic signal generated in the sample is collected through the objective 1. After filtering with a short-pass filter to remove the remnants of the fundamental wave, the sample is imaged with a CCD camera. (b) Optical image of the photonic structure and close-up SEM images of its main components: the grating coupler (circled with blue), single-mode and structured waveguides (circled with green), and coupled waveguide lattice (circled with red). (c–h) Propagation of topological edge modes and bulk modes for different excitation wavelengths visualized via third harmonic signal. (c–e) Excitation through coupler 1 (edge mode regime). (f–h) Excitation through coupler 2 (bulk mode regime). Red dashed lines in (c–h) show the contours of the structure.

https://doi.org/10.1021/acs.nanolett.2c04182
Nano Lett. 2023, 23, 2094−2099

In agreement with our theoretical model and simulations, the coupling of light through coupler 1 leads to the excitation of a topological edge mode, which manifests itself as a strong third harmonic signal localized at the edge of the waveguide array (Figure 4c–e). In contrast, excitation through the coupler 2 reverses the phase difference between the modes of the extended waveguide, which causes the diffraction of waves into the bulk of the array (Figure 4f–h). The topological edge mode emerges in the range of wavelengths from 1530 to 1600 nm, consistent with our numerical results; the localization of the edge mode at wavelength of 1560 nm appears to be especially pronounced (Figure 4d), which indicates the optimal combination of the directional coupler efficiency and the proximity to the degeneracy point of the two waveguide modes. As illustrated in Figure S5, in this case the propagation length of the edge mode at 1560 nm reaches 27 μm. The observed inhomogeneity of the THG signal along the edge is a combined effect of scattering from the directional coupler, local defects of the structure, and back-reflection of the edge mode, which is further enhanced by the nonlinear frequency conversion process used for detection. Notably, the third harmonic signal from the waveguide array decreases with the increase of the detuning between the propagation constants of the waveguide, which is mostly due to the limited bandwidth of the directional coupler. A more detailed spectral dependence of the THG images with color scales optimized independently for each wavelength is presented in Figure S6. Even larger detunings of the excitation from the degeneracy point cause closing of the topological gap. In this regime, bulk modes are excited both when the structure is fed through coupler 1 or coupler 2. This trivial case is illustrated in Figure S7.

These experimental results confirm the emergence of topological edge state mediated by the accidental degeneracy of the modes of the individual waveguide. Hybrid nature of the edge state enables its coherent control and the possibility to continuously tune the operation of the structure from bulk to edge modes. At the same time, the degree of the edge mode localization is controlled by the excitation wavelength. Thus, the designed setup uncovers novel possibilities of integrated photonic topological structures extending the range of their possible functionalities.

In conclusion, our experiments demonstrate a novel avenue to design highly controllable topological insulator structures and meta-devices at the nanoscale. Owing to the multimode nature of the lattice, the observed topological modes have hybrid nature exhibiting different excitation efficiencies for the different input ports of the optical signal. This feature gives an immediate access to their coherent control and switching in real-time.

At the same time, the topological properties of our structure can be manipulated by changing the wavelength of excitation which determines not only the localization length but also the very existence of the topological edge mode. We believe that the proposed strategy could be also beneficial for other classes of topological meta-devices such as topological waveguides, cavities, and lasers.

■ ASSOCIATED CONTENT

Supporting Information

The Supporting Information is available free of charge at https://pubs.acs.org/doi/10.1021/acs.nanolett.2c04182.

Fabrication and optical characterization methods; tight-binding analysis of the designed structure including the derivation of the topological properties; optimization of a single waveguide to achieve the degeneracy of its modes with the different symmetry of the near field and efficiently excite these modes through a directional coupler; more detailed discussion of the experimental data and estimate of the propagation length for the edge modes in the designed array (PDF)

■ AUTHOR INFORMATION

Corresponding Author

Maxim A. Gorlach − *School of Physics and Engineering, ITMO University, Saint Petersburg 197101, Russia;* orcid.org/0000-0002-7880-8953; Email: m.gorlach@metalab.ifmo.ru

Authors

Alexey O. Mikhin − *School of Physics and Engineering, ITMO University, Saint Petersburg 197101, Russia*

Viktoriia Rutckaia − *Photonics Initiative, Advanced Science Research Center, The City University of New York, New York, New York 10031, United States; Centre for Innovation Competence SiLi-nano, Martin-Luther-University, 06120 Halle (Saale), Germany*

Roman S. Savelev − *School of Physics and Engineering, ITMO University, Saint Petersburg 197101, Russia;* orcid.org/0000-0002-7810-960X

Ivan S. Sinev − *School of Physics and Engineering, ITMO University, Saint Petersburg 197101, Russia;* orcid.org/0000-0002-4246-7747

Andrea Alù − *Photonics Initiative, Advanced Science Research Center, The City University of New York, New York, New York 10031, United States; Physics Program, Graduate Center, The City University of New York, New York, New York 10016, United States;* orcid.org/0000-0002-4297-5274

Complete contact information is available at: https://pubs.acs.org/10.1021/acs.nanolett.2c04182

Author Contributions

A.O.M., V.R., and R.S.S. contributed equally to this work.

Notes

The authors declare no competing financial interest.

■ ACKNOWLEDGMENTS

We acknowledge Maxim Mazanov and Prof. Rodrigo Vicencio for valuable discussions. Theoretical and numerical studies were supported by Priority 2030 Federal Academic Leadership Program and Russian Science Foundation (Grant 20-72-10065), respectively. Optical characterization of the structure was supported by the Ministry of Science and Higher Education of the Russian Federation (Project 075-15-2021-589). Sample fabrication and initial characterization were supported by the Air Force Office of Scientific Research, the Simons Foundation and the European Union's Horizon 2020 research and innovation programme under the Marie Sklodowska-Curie Grant Agreement N 845287. M.A.G. acknowledges partial support by the Foundation for the Advancement of Theoretical Physics and Mathematics "Basis".

REFERENCES

(1) Lu, L.; Joannopoulos, J. D.; Soljačić, M. Topological photonics. *Nat. Photonics* **2014**, *8*, 821−829.
(2) Lu, L.; Joannopoulos, J. D.; Soljačić, M. Topological states in photonic systems. *Nat. Phys.* **2016**, *12*, 626−629.
(3) Ozawa, T.; Price, H. M.; Amo, A.; Goldman, N.; Hafezi, M.; Lu, L.; Rechtsman, M. N.; Schuster, D.; Simon, J.; Zilberberg, O.; Carusotto, I. Topological photonics. *Rev. Mod. Phys.* **2019**, *91*, 015006.
(4) Raghu, S.; Haldane, F. D. M. Analogs of quantum-Hall-effect edge states in photonic crystals. *Phys. Rev. A* **2008**, *78*, 033834.
(5) Haldane, F. D. M.; Raghu, S. Possible Realization of Directional Optical Waveguides in Photonic Crystals with Broken Time-Reversal Symmetry. *Phys. Rev. Lett.* **2008**, *100*, 013904.
(6) Wang, Z.; Chong, Y.; Joannopoulos, J. D.; Soljačić, M. Observation of unidirectional backscattering-immune topological electromagnetic states. *Nature* **2009**, *461*, 772−775.
(7) Rechtsman, M. C.; Zeuner, J. M.; Plotnik, Y.; Lumer, Y.; Podolsky, D.; Dreisow, F.; Nolte, S.; Segev, M.; Szameit, A. Photonic Floquet topological insulators. *Nature* **2013**, *496*, 196−200.
(8) Hafezi, M.; Demler, E. A.; Lukin, M. D.; Taylor, J. M. Robust optical delay lines with topological protection. *Nat. Phys.* **2011**, *7*, 907−912.
(9) Hafezi, M.; Mittal, S.; Fan, J.; Migdall, A.; Taylor, J. M. Imaging topological edge states in silicon photonics. *Nat. Photonics* **2013**, *7*, 1001−1005.
(10) Khanikaev, A. B.; Mousavi, S. H.; Tse, W. K.; Kargarian, M.; MacDonald, A. H.; Shvets, G. Photonic topological insulators. *Nat. Mater.* **2013**, *12*, 233.
(11) Wu, L.-H.; Hu, X. Scheme for Achieving a Topological Photonic Crystal by Using Dielectric Material. *Phys. Rev. Lett.* **2015**, *114*, 223901.
(12) Yves, S.; Fleury, R.; Berthelot, T.; Fink, M.; Lemoult, F.; Lerosey, G. Crystalline metamaterials for topological properties at subwavelength scales. *Nat. Commun.* **2017**, *8*, 16023.
(13) Barik, S.; Karasahin, A.; Flower, C.; Cai, T.; Miyake, H.; DeGottardi, W.; Hafezi, M.; Waks, E. A topological quantum optics interface. *Science* **2018**, *359*, 666−668.
(14) Li, Y.; Sun, Y.; Zhu, W.; Guo, Z.; Jiang, J.; Kariyado, T.; Chen, H.; Hu, X. Topological LC-circuits based on microstrips and observation of electromagnetic modes with orbital angular momentum. *Nat. Commun.* **2018**, *9*, 4598.
(15) Gorlach, M. A.; Ni, X.; Smirnova, D. A.; Korobkin, D.; Zhirihin, D.; Slobozhanyuk, A. P.; Belov, P. A.; Alù, A.; Khanikaev, A. B. Far-field probing of leaky topological states in all-dielectric metasurfaces. *Nat. Commun.* **2018**, *9*, 909.
(16) Noh, J.; Benalcazar, W. A.; Huang, S.; Collins, M. J.; Chen, K. P.; Hughes, T. L.; Rechtsman, M. C. Topological protection of photonic mid-gap defect modes. *Nat. Photonics* **2018**, *12*, 408−415.
(17) Yang, Y.; Xu, Y. F.; Xu, T.; Wang, H.-X.; Jiang, J.-H.; Hu, X.; Hang, Z. Visualization of a Unidirectional Electromagnetic Waveguide Using Topological Photonic Crystals Made of Dielectric Materials. *Phys. Rev. Lett.* **2018**, *120*, 217401.
(18) Smirnova, D.; Kruk, S.; Leykam, D.; Melik-Gaykazyan, E.; Choi, D.-Y.; Kivshar, Y. Third-Harmonic Generation in Photonic Topological Metasurfaces. *Phys. Rev. Lett.* **2019**, *123*, 103901.
(19) Parappurath, N.; Alpeggiani, F.; Kuipers, L.; Verhagen, E. Direct observation of topological edge states in silicon photonic crystals: Spin, dispersion, and chiral routing. *Sci. Adv.* **2020**, *6*, eaaw4137.
(20) Poddubny, A.; Miroshnichenko, A.; Slobozhanyuk, A.; Kivshar, Y. Topological Majorana States in Zigzag Chains of Plasmonic Nanoparticles. *ACS Photonics* **2014**, *1*, 101−105.
(21) Sinev, I. S.; Mukhin, I. S.; Slobozhanyuk, A. P.; Poddubny, A. N.; Miroshnichenko, A. E.; Samusev, A. K.; Kivshar, Y. S. Mapping plasmonic topological states at the nanoscale. *Nanoscale* **2015**, *7*, 11904−11908.
(22) Slobozhanyuk, A. P.; Poddubny, A. N.; Miroshnichenko, A. E.; Belov, P. A.; Kivshar, Y. S. Subwavelength Topological Edge States in Optically Resonant Dielectric Structures. *Phys. Rev. Lett.* **2015**, *114*, 123901.
(23) Solnyshkov, D. D.; Nalitov, A. V.; Malpuech, G. Kibble-Zurek Mechanism in Topologically Nontrivial Zigzag Chains of Polariton Micropillars. *Phys. Rev. Lett.* **2016**, *116*, 046402.
(24) Kruk, S.; Poddubny, A.; Smirnova, D.; Wang, L.; Slobozhanyuk, A.; Shorokhov, A.; Kravchenko, I.; Luther-Davies, B.; Kivshar, Y. Nonlinear light generation in topological nanostructures. *Nat. Nanotechnol.* **2019**, *14*, 126−130.
(25) St-Jean, P.; Goblot, V.; Galopin, E.; Lemaitre, A.; Ozawa, T.; Le Gratiet, L.; Sagnes, I.; Bloch, J.; Amo, A. Lasing in topological edge states of a one-dimensional lattice. *Nat. Photonics* **2017**, *11*, 651−656.
(26) Ezawa, M. Higher-Order Topological Insulators and Semimetals on the Breathing Kagome and Pyrochlore Lattices. *Phys. Rev. Lett.* **2018**, *120*, 026801.
(27) Xue, H.; Yang, Y.; Gao, F.; Chong, Y.; Zhang, B. Acoustic higher-order topological insulator on a kagome lattice. *Nat. Mater.* **2019**, *18*, 108−112.
(28) Ni, X.; Weiner, M.; Alù, A.; Khanikaev, A. B. Observation of higher-order topological acoustic states protected by generalized chiral symmetry. *Nat. Mater.* **2019**, *18*, 113−120.
(29) Cáceres-Aravena, G.; Torres, L. E. F. F.; Vicencio, R. A. Topological and flat-band states induced by hybridized linear interactions in one-dimensional photonic lattices. *Phys. Rev. A* **2020**, *102*, 023505.
(30) Savelev, R. S.; Gorlach, M. A. Topological states in arrays of optical waveguides engineered via mode interference. *Phys. Rev. B* **2020**, *102*, 161112.
(31) Guzmán-Silva, D.; Cáceres-Aravena, G.; Vicencio, R. A. Experimental Observation of Interorbital Coupling. *Phys. Rev. Lett.* **2021**, *127*, 066601.
(32) Warren, W.; Rabitz, H.; Dahleh, M. Coherent control of quantum dynamics: the dream is alive. *Science* **1993**, *259*, 1581−1589.
(33) Goswami, D. Optical pulse shaping approaches to coherent control. *Phys. Rep.* **2003**, *374*, 385−481.
(34) Rabitz, H. Focus on quantum control. *New J. Phys.* **2009**, *11*, 105030.
(35) Zhang, Z.; Kang, M.; Zhang, X.; Feng, X.; Xu, Y.; Chen, X.; Zhang, H.; Xu, Q.; Tian, Z.; Zhang, W.; Krasnok, A.; Han, J.; Alù, A. Coherent Perfect Diffraction in Metagratings. *Adv. Mater.* **2020**, *32*, 2002341.
(36) Kang, M.; Zhang, Z.; Wu, T.; Zhang, X.; Xu, Q.; Krasnok, A.; Han, J.; Alù, A. Coherent full polarization control based on bound states in the continuum. *Nat. Commun.* **2022**, *13*, 1−9.
(37) Yuan, L.; Lin, Q.; Xiao, M.; Fan, S. Synthetic dimension in photonics. *Optica* **2018**, *5*, 1396.
(38) Lustig, E.; Weimann, S.; Plotnik, Y.; Lumer, Y.; Bandres, M. A.; Szameit, A.; Segev, M. Photonic topological insulator in synthetic dimensions. *Nature* **2019**, *567*, 356−360.
(39) Cheben, P.; Halir, R.; Schmid, J. H.; Atwater, H. A.; Smith, D. R. Subwavelength integrated photonics. *Nature* **2018**, *560*, 565−572.
(40) Johnson, S. G.; Ibanescu, M.; Skorobogatiy, M. A.; Weisberg, O.; Joannopoulos, J. D.; Fink, Y. Perturbation theory for Maxwell's equations with shifting material boundaries. *Phys. Rev. E* **2002**, *65*, 066611.

https://doi.org/10.1021/acs.nanolett.2c04182
Nano Lett. 2023, 23, 2094−2099